Supporting Information

Two-Photon Dual-Emissive Carbon Dot-Based Probe: Deep Tissue Imaging and Ultrasensitive Sensing of Intracellular Ferric Ions

Pooria Lesani,[†,‡] Gurvinder Singh,[†,‡] Christina Marie Viray,[†,‡] Yogambha Ramaswamy,[†,‡] De Ming Zhu,[§] Peter Kingshott,[§,ζ] Zufu Lu,[†,‡] Hala Zreiqat*[,†,‡]*

[†] Tissue Engineering & Biomaterials Research Unit, School of Biomedical Engineering, and [‡] ARC Training Centre for Innovative BioEngineering, The University of Sydney, Sydney, NSW 2006, Australia

[§] Department of Chemistry and Biotechnology, School of Science, Swinburne University of Technology, Hawthorn, Victoria 3122, Australia

[ζ] ARC Training Centre Training Centre in Surface Engineering for Advanced Materials (SEAM), School of Engineering, Swinburne University of Technology, Hawthorn, Victoria 3122, Australia

Corresponding Authors: zufu.lu@sydney.edu.au, hala.zreiqat@sydney.edu.au

Supplementary Tables

1. XPS Analysis

Table S1. Surface atomic percentage of CDs from XPS.

Sample	%C1s	%N1s	%O1s
1-CDs	66.0	15.1	18.9
2-CDs	67.9	14.7	17.4
3-CDs	66.9	15.0	18.1

2. Quantum Yield Comparison

Table S2. Quantum yield comparison of the carbon dots synthesized in this work with recently reported carbon dots probes.

Synthetic sources	Quantum Yield (%)	Ref.
Sodium alginate	~ 2.0	1
Leeks	5.6	2
Ascorbic acid, glycol	5.7	3
1,2,4-Triaminobenzen	10.8	4
Rose flowers	13.45	5
P-phenylenediamine	14.0	6
P. Acidus	14.0	7
Aspartic acid, NH_4HCO_3	14.0	6
Wool	16.3	8
Amino salicylic acid	16.4	9
Diethylamine, $CHCl_3$	17.1	10
CCl_4, $NaNH_2$	22.0	11
Malic Acid	30.0	12
Ascorbic acid, Arginine	22.8 - 36.5 (based on the CDs size distribution)	This Work

Table S3. Comparison of 3-FCDs two-photon fluorescence imaging features with the recently reported fluorescence probes

Probe	TPF tissue imaging	Tissue incubation time (h)	Maximum penetration depth (μm)	TPF cell imaging	Ref.
4′-(Aminomethylphenyl) 2,2′:6′,2″-terpyridine conjugated carbon dots	Biological tissue imaging (lung cancer and LLC-MK2 cells tumor tissue)	6	185	Lung cancer cells	13
Nitrogen-doped graphene quantum dots	Synthetic tissue imaging (Tissue Phantom)	-	1800	Hela cells	14
Carbon dots	-	-	-	Hela cells	15
Carbon dots	-	-	-	Breast cancer cells	16
Carbon dots	-	-	-	-	17
PEG-Chitosan@carbon dots	-	-	-	Prostate cancer cells	18
FITC conjugated CDs (This work)	Biological tissue imaging (Pigskin tissue)	3	280	Fibroblast skin cells	-
	Synthetic tissue (hydrogel scaffold)		3000		

Supplementary Figures

1. XPS Analysis

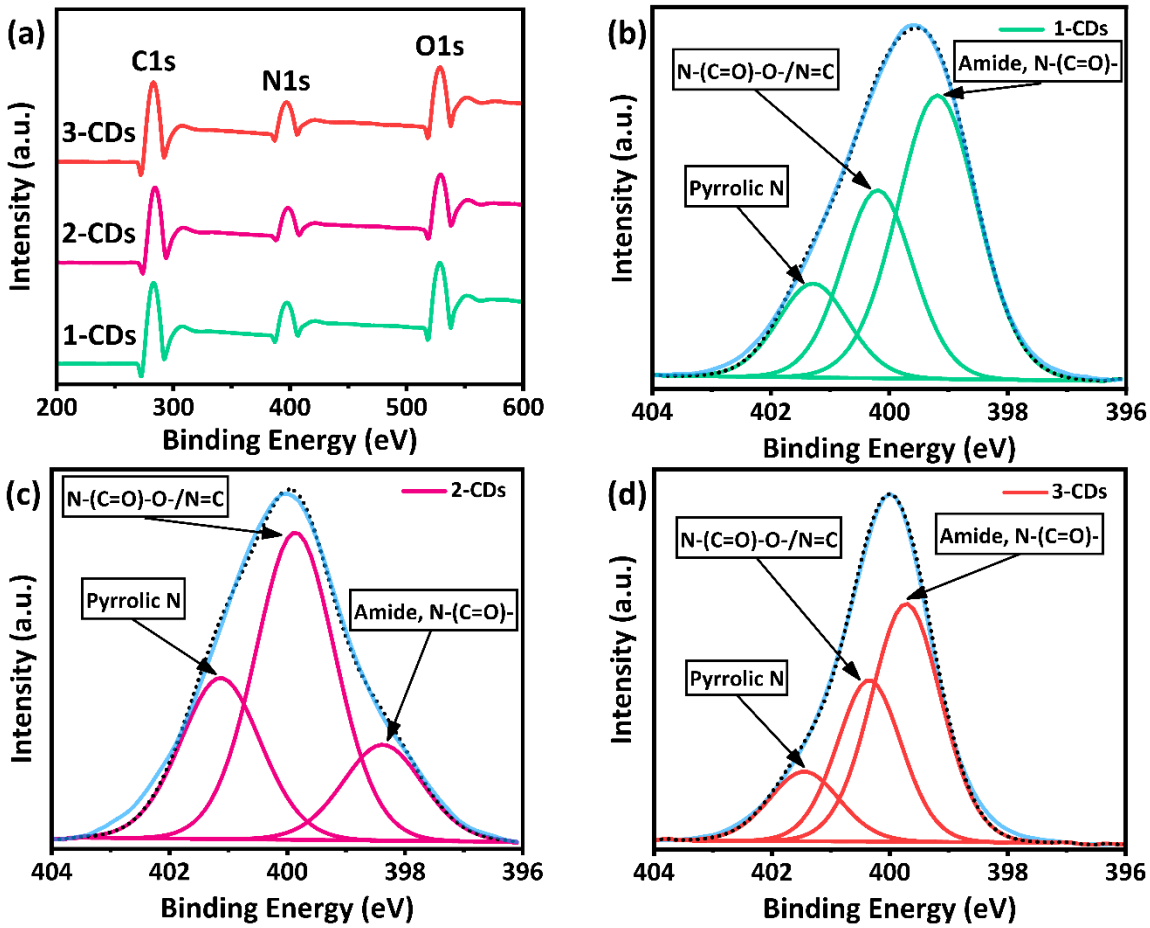

Figure S1. XPS survey spectra (a), and detailed N1s spectra (b-d) of 1-CDs, 2-CDs, and 3-CDs, respectively.

2. Photostability

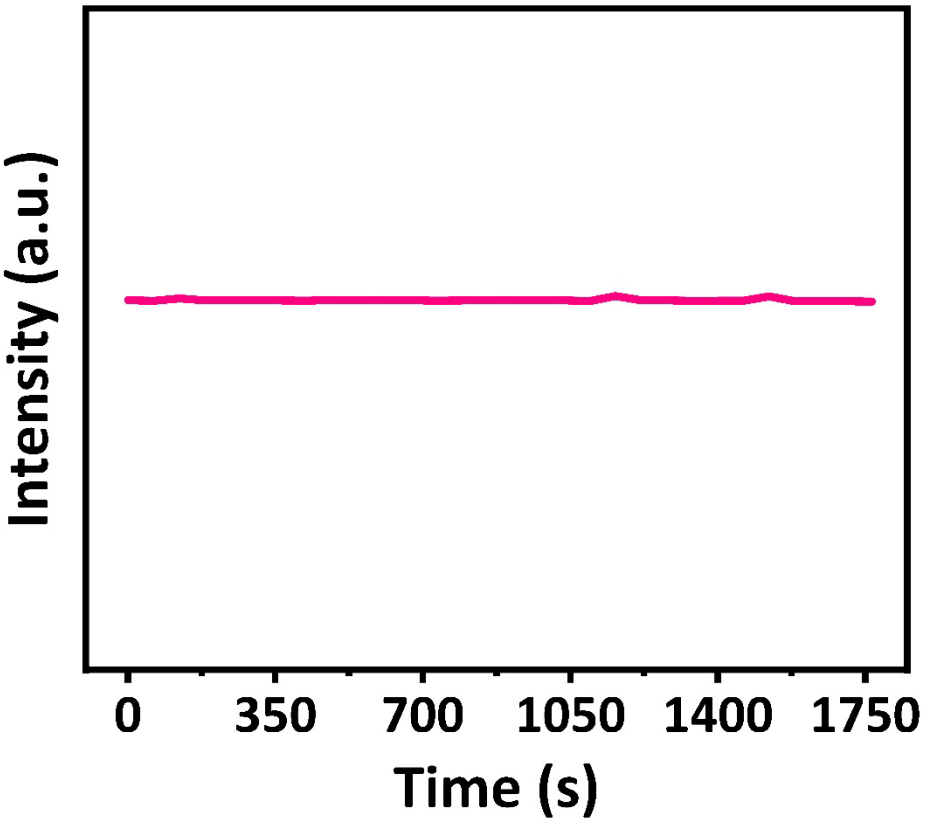

Figure S2. Photostability test of 3-FCDs under continuous irradiation with a two-photon NIR laser at excitation wavelength of 750 nm.

3. Single-Photon Fluorescence Deep-Tissue Imaging

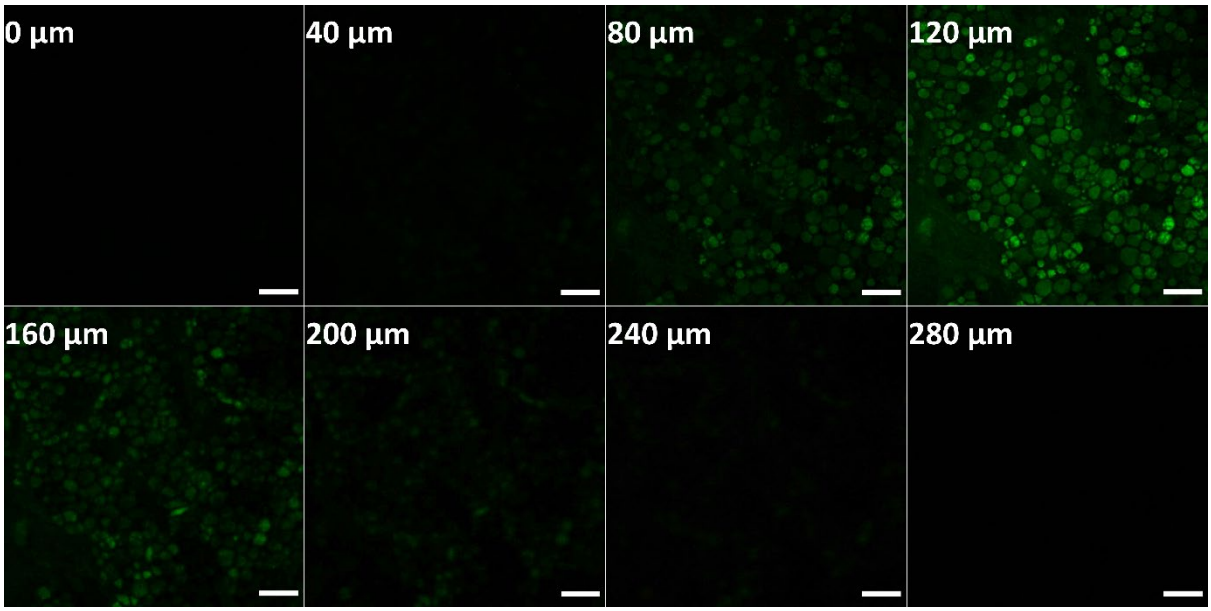

Figure S3. Single-photon excited Z-stack images of pigskin tissue after incubation with 3-FCDs (300 µg/mL) for 3 h (from 0 to 280 µm; Δz = 40 µm, scale: 200 µm).

4. Bare 3-CDs and FITC Sensitivity Towards Fe^{3+}

We have also studied the Fe^{3+} sensing capability of bare 3-CDs and FITC, separately. As it is shown in Figure S4a and c, no significant fluorescence quenching was observed in pure FITC and 3-CDs solution in the presence of ferric ions with concentration up to 2.5 and 0.5 μM, respectively. The first noticeable fluorescence quenching of FITC and 3-CDs occurred at 10 and 1 μM concentration of ferric ions. The FITC and 3-CDs fluorescence intensity ratio (I/I_0) as a function of Fe^{3+} concentration is presented in Figure S4b and d. The I/I_0 ratio for both the FITC and 3-CDs displayed a non-linear plotting with the fluttered trend at low concentration of ferric ions (0-2.5 μM) with a detection limit of 0.433 and 0.151 μM, respectively (based on the ratio of the standard deviation of the response to the profile slope, $3\sigma/S$). Also, the fluorescence quenching efficiency of 53.5% and 52.7% at the concentration of 500 μM Fe^{3+} was observed for both FITC and 3-CDs, respectively. On the contrary, the conjugated FITC molecules and 3-CDs work synergistically to improve the detection limit and sensitivity of the 3-FCDs probe in detecting ferric ions. A notable fluorescence quenching of 3-FCDs was noticed upon the addition of Fe^{3+} with the concentration of 1.6 μM. The fluorescence quenching efficiency of the 3-FCDs increases up to 65.1 and 62.8% for both 3-CDs and FITC (FITC conjugated 3-CDs) at 500 μM Fe^{3+}, respectively (Figure 7e). Surprisingly, the 3-FCDs show a linear relationship in the range of 0 to 20 μM with an extraordinary detection limit of 1.56 nM. Therefore, the results discussed above clearly demonstrate a significantly improved the ferric ion sensing ability of 3-FCDs compared to FITC or 3-CDs. Also, we investigated the effect of CDs size on sensing performance. The results exhibited approximately similar sensitivity limit value of 1-CDs (0.163 μM), 2-CDs (0.142 μM), and 3-CDs (0.151 μM) for ferric ion detection. This is because of similar surface functionality of different CDs sizes (Figure 2 and S1).

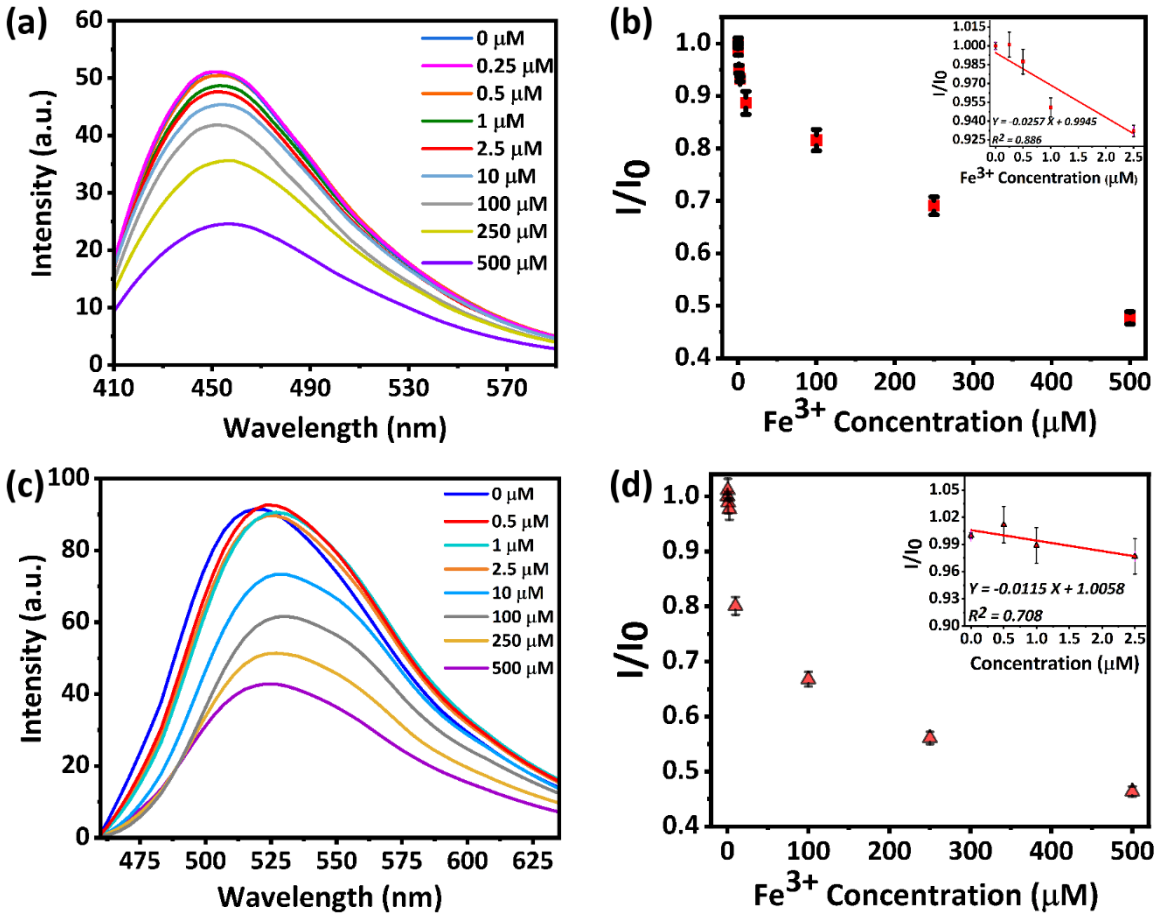

Figure S4. (a, c) Fluorescence spectra of the 3-CDs and FITC before and after addition of different concentrations of Fe^{3+}, and (b, d) fluorescence intensity ratio I/I_0 (obtained from Figure S4a and b) as a function of Fe^{3+} concentration, respectively (Insets: fluorescence intensity ratio I/I_0 as a function of Fe^{3+} concentration in the range of 0-2.5 μM, respectively).

5. Complexation Between FITC and Fe^{3+}

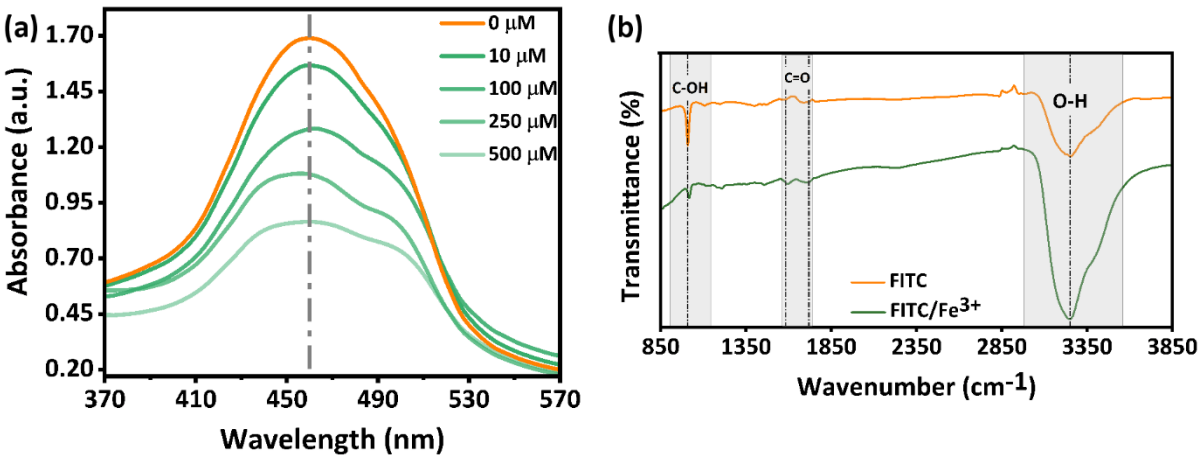

Figure S5. (a) UV-vis absorption, and (b) FT-IR spectra of FITC before and after addition of Fe^{3+} ions.

6. 3-CDs, FITC, and 3-FCDs Response Time

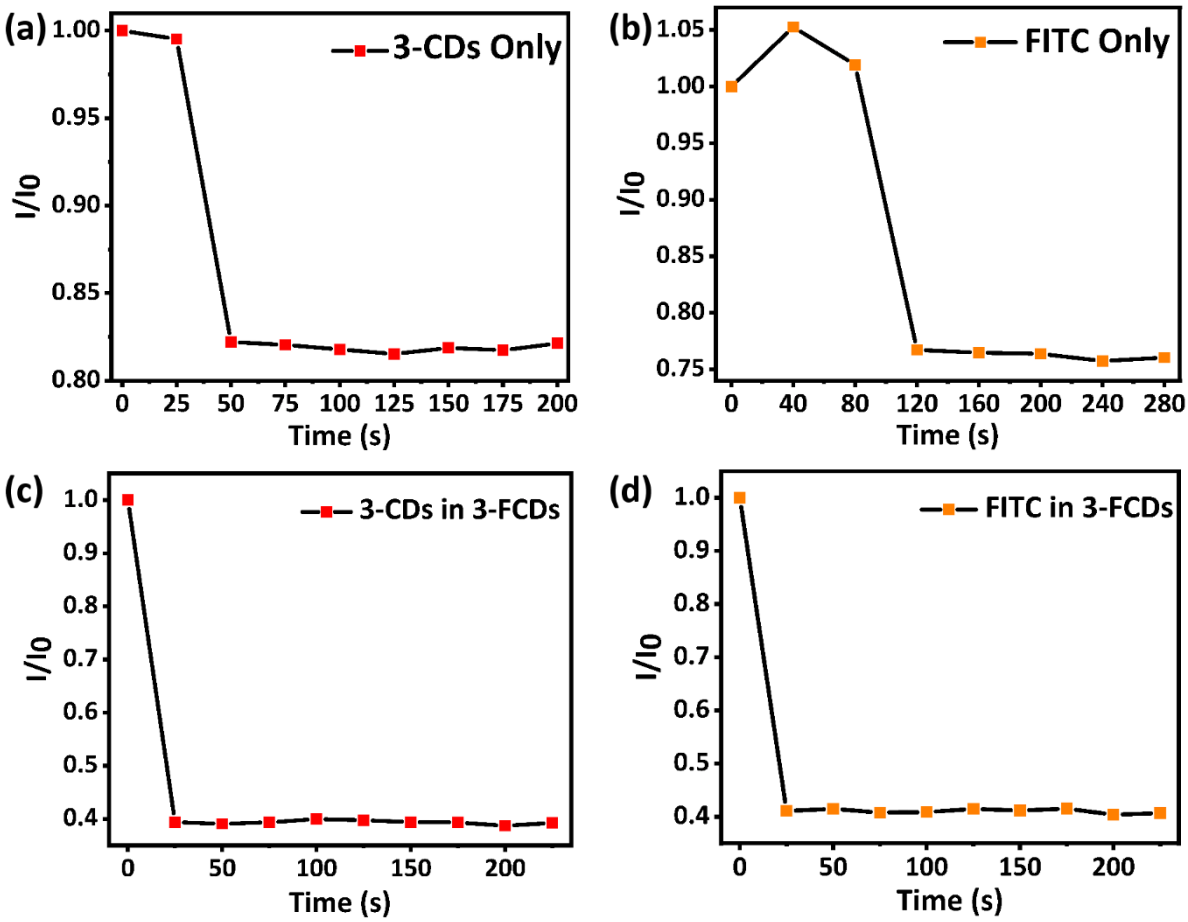

Figure S6. The response time of (a) bare 3-CDs, (b) bare FITC, (c) 3-CDs in 3-FCDs, and (d) FITC in 3-FCDs toward the addition of 500 μM Fe^{3+}.

7. Cell Viability

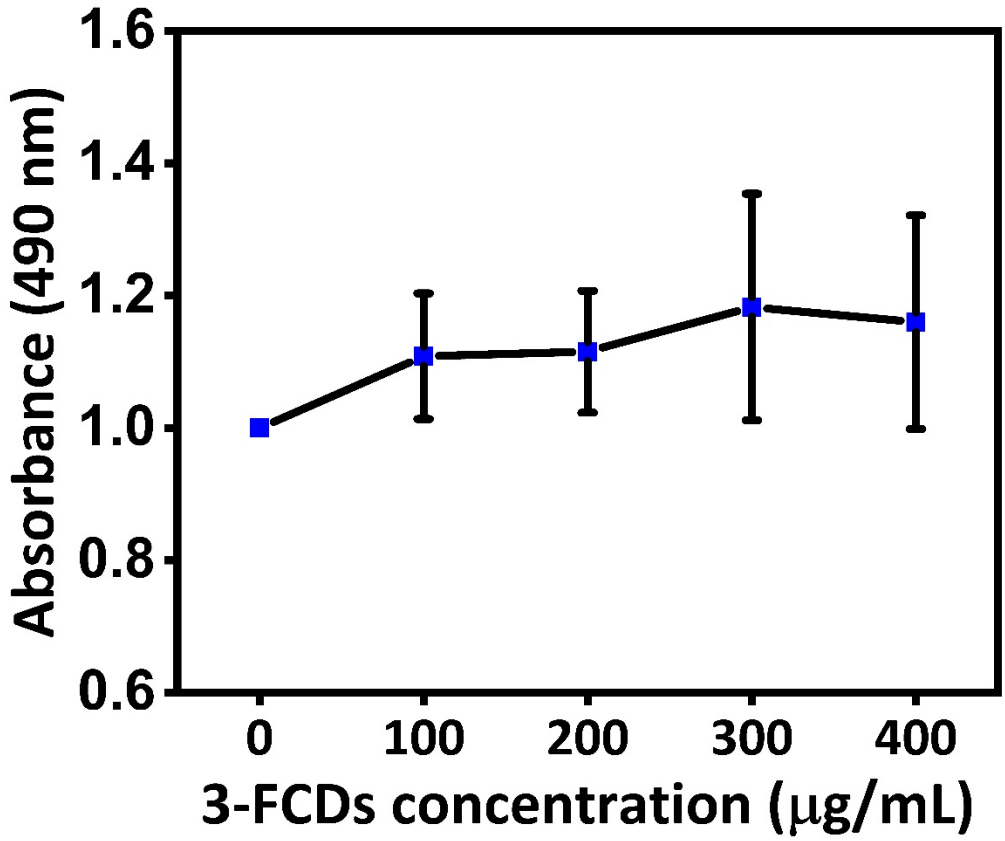

Figure S7. Cytotoxic effects of 3-FCDs on skin fibroblast cells at increasing concentration for 72 h (mean ± SD, n = 3). Cells incubated with only media as control.

8. Two-Photon Fluorescence Cell Imaging

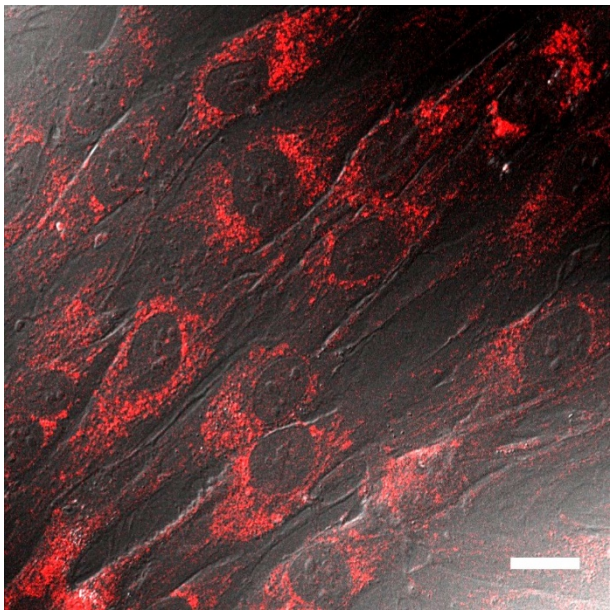

Figure S8. Overlay of DIC and two-photon fluorescence images of fibroblast skin cells incubated with 300 μg/mL 3-FCDs for 24 h (scale: 20 μm).

9. Two-Photon Fluorescence Imaging and Mean Fluorescence Intensity of Fibroblasts Before and After AA Addition

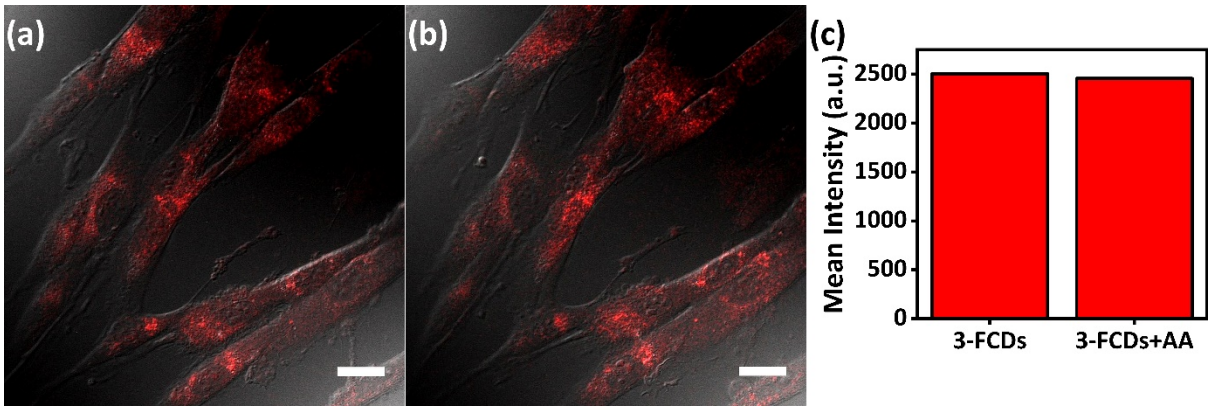

Figure S9. Two-photon fluorescence images of fibroblast after incubation with 300 μg/mL of 3-FCDs for 24 h and then 1 mM Ascorbic Acid (AA) for (a) 0 h, and (b) 1 h. (c) Mean fluorescence intensity of cells incubated with 3-FCDs and 3-FCDs+AA (scale: 20 μm).

10. The Average Fluorescence Ratio Versus the LPS Treatment Time

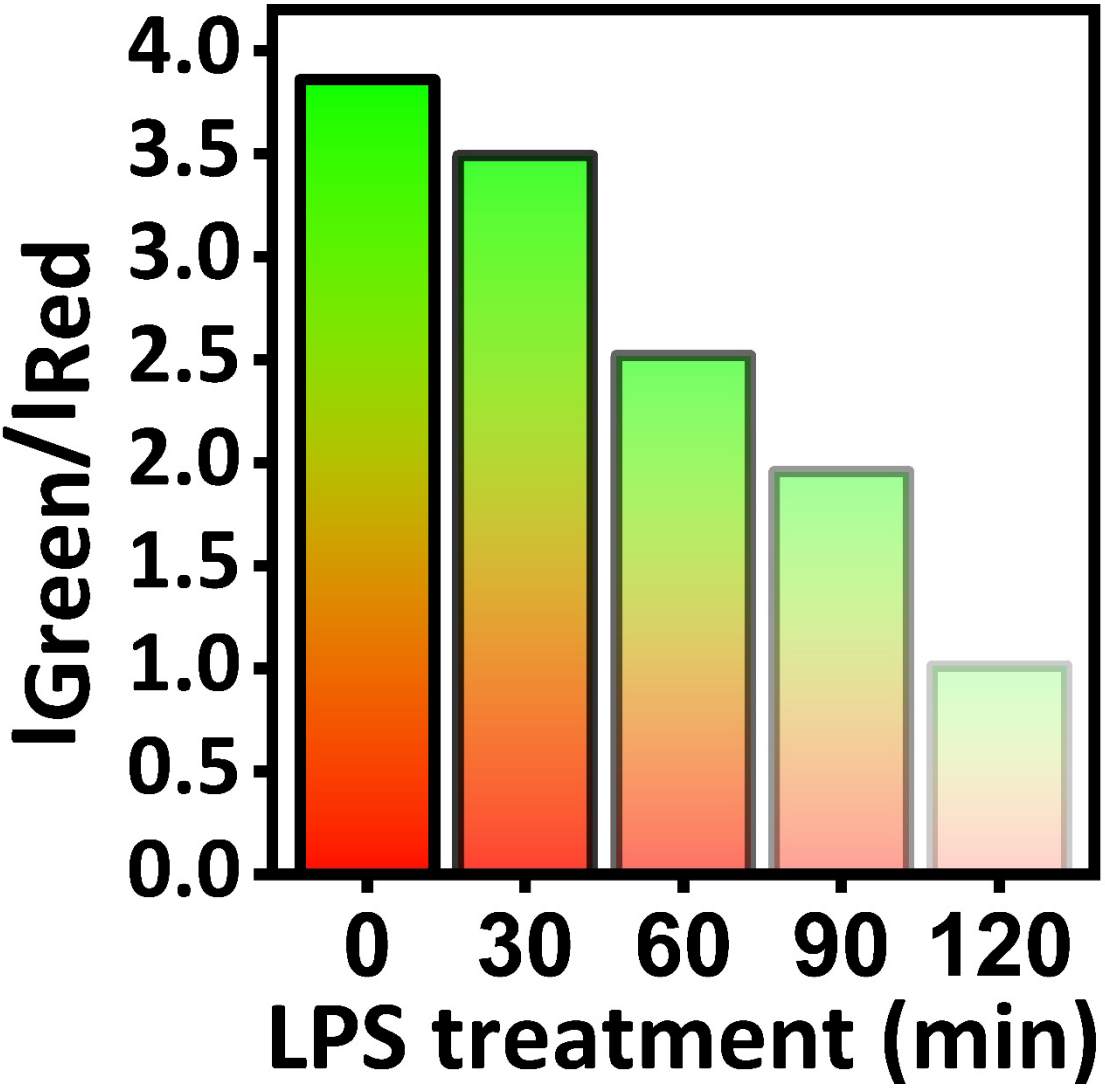

Figure S10. The average fluorescence ratio I_{Green}/I_{Red} (from 15 cells calculated using ImageJ software) versus the LPS treatment time.

Supplementary Videos

1. The Z-axis Imaging

Z-stack, Fibroblast Skin Cells Incubated with 3-FCDs.avi

Video S1. The video shows the Z-stack of cells incubated with 3-FCDs at different Z positions.

Extra Studies:

Fabrication of pH Test Strips with 3-FCDs

First, we cut the cellulose-based filter paper into circles with a diameter of 0.6 cm. Next, a series of 20 μL solutions containing the dual-emissive 3-FCDs (300 μg/mL) were transferred onto the prepared filter papers and kept in the dark for 30 min to obtain a uniform paper sensor. The solutions with pH values of 5, 6, 7, and 8 were pipetted onto the as-prepared paper sensors. A digital camera recorded the fluorescence changes under irradiation with a 365 nm UV lamp.

Dual-Emissive pH Sensing

To investigate the capability of 3-FCDs for pH sensing, the fluorescence intensity of the probe was analysed in the pH range of 4.1 to 10.0. Figure S8a shows that at both peaks of fluorescence intensity at 445 nm (I_{Red}) and 515 nm (I_{Green}) was increased by changing the pH value from 4.1 to 10.0, with no obvious change in peak position under the excitation wavelength of 390 nm. This phenomenon can be attributed to the protonation and deprotonation of the functional groups (such as amino and carboxyl groups) existing on the surface of the probe [6]. Figure S8b shows ratiometric intensities (I_{Green}/I_{Red}) of 3-FCDs at the maximum emission peaks of CDs and FITC at different pH values and the inset which shows the linear response of the probe to pH changes in the range of 5.6-7.5.

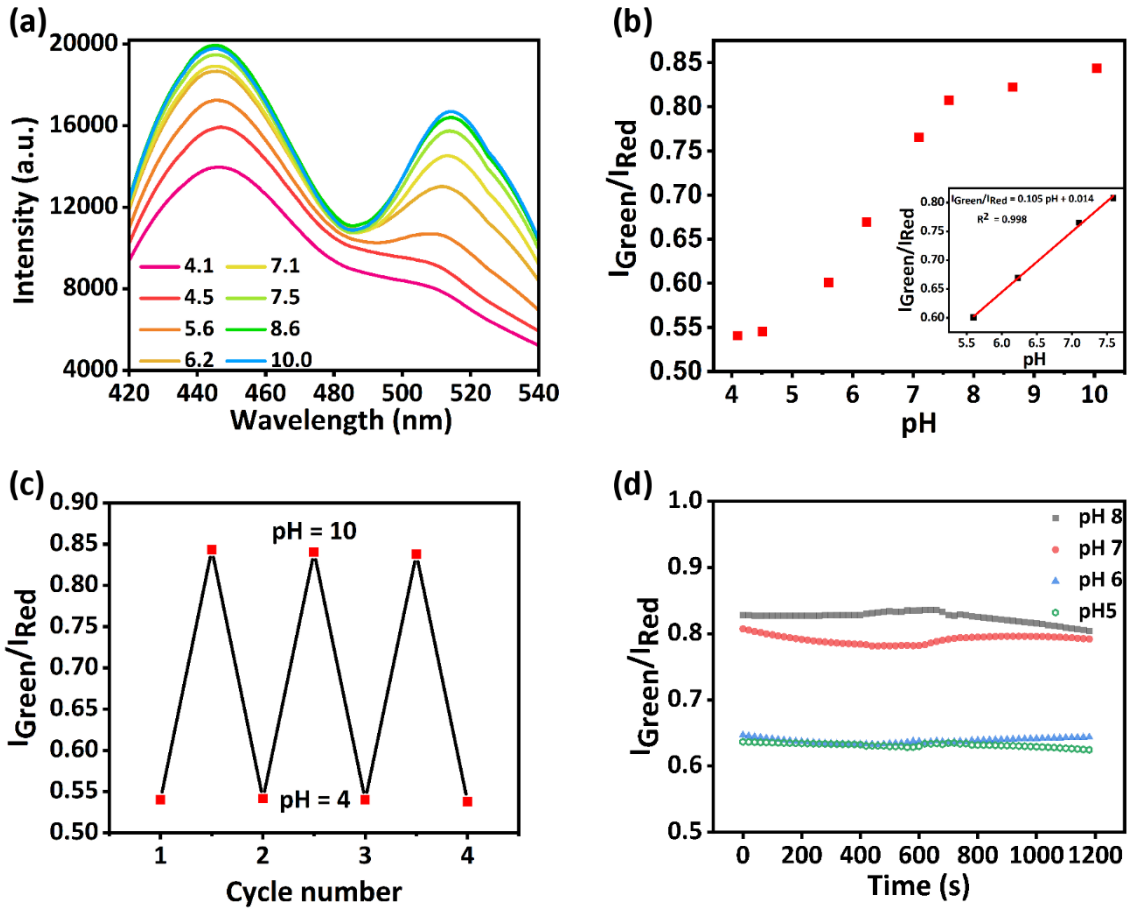

Figure S11. (a) PL emission spectra of 3-FCDs at pH ranging from 4.1 to 10.0, (b) Ratiometric PL intensities (I_{Green}/I_{Red}) of 3-FCDs at the maximum emission peaks at different pH values. Inset: linear plotting of I_{Green}/I_{Red} versus pH. (c) Fluorescence reversibility of 3-FCDs between pH 4 and 10, (d) Photostability test of 3-FCDs at different pH values under continuous irradiation with UV light (500 W).

Interestingly, the fluorescence emitting color of the 3-FCDs aqueous solution altered from deep-blue to deep-green by changing the pH from 5 to 8 (Figure S9a). Therefore, we utilized the 3-FCDs pH sensitivity advantage for on-site and rapid determination of pH values. For this purpose, a paper-based sensor was developed. In detail, a series of 20 µL 3-FCDs solution (300 µ/mL) were transferred onto the pieces of filter papers (6 mm in diameter) and then kept in the dark for 30 min to achieve uniform paper sensors. Under UV-lamp, the as-prepared papers showed a cyan fluorescence color, Figure S9b (the raw paper was non-fluorescent). Next, 20

μL of the solutions with a pH value of 5, 6, 7, and 8 were transferred onto the paper sensors. As clearly observed by the naked eye, the color of the paper-based sensor changed from deep-blue to cyan, light green, and deep-green by increasing the pH value from 5 to 8 (Figure S9c). The results mentioned above and Figure S9c shows the promising applicability of the paper-based sensor for the visual detection of pH.

Also, the reversibility of the 3-FCDs was investigated at different pH values (5 to 8). As shown in Figure S8c, the pH value switched from pH 5 to pH 8 four times with no obvious changes in fluorescence intensity which indicates the high pH-reversibility of the 3-FCDs. Furthermore, the photostability of 3-FCDs at different pH values was tested under continued irradiation with UV light (500 W) for 1200 s, and no significant changes were observed (Figure S8d).

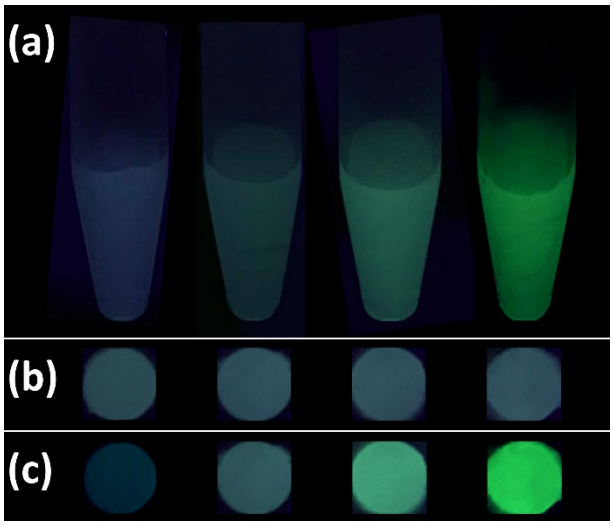

Figure S12. (a) Fluorescence images of the aqueous suspension of 3-FCDs at different pH values. The images of the paper-based sensor (b) after addition of 3-FCDs, followed by (c) addition of the solutions with different pH values under a 365 nm UV lamp. pH values from left to right: 5, 6, 7, and 8.

REFERENCES

(1) Fong, J. F. Y.; Chin, S. F.; Ng, S. M. A unique "turn-on" fluorescence signalling strategy for highly specific detection of ascorbic acid using carbon dots as sensing probe. *Biosensors and Bioelectronics* **2016,** *85*, 844-852.

(2) Shi, L.; Li, Y.; Li, X.; Zhao, B.; Wen, X.; Zhang, G.; Dong, C.; Shuang, S. Controllable synthesis of green and blue fluorescent carbon nanodots for pH and Cu^{2+} sensing in living cells. *Biosensors and Bioelectronics* **2016,** *77*, 598-602.

(3) Wu, H.; Mi, C.; Huang, H.; Han, B.; Li, J.; Xu, S. Solvothermal synthesis of green-fluorescent carbon nanoparticles and their application. *Journal of Luminescence* **2012,** *132* (6), 1603-1607.

(4) Jiang, K.; Sun, S.; Zhang, L.; Wang, Y.; Cai, C.; Lin, H. Bright-yellow-emissive N-doped carbon dots: preparation, cellular imaging, and bifunctional sensing. *ACS applied materials & interfaces* **2015,** *7* (41), 23231-23238.

(5) Feng, Y.; Zhong, D.; Miao, H.; Yang, X. Carbon dots derived from rose flowers for tetracycline sensing. *Talanta* **2015,** *140*, 128-133.

(6) Zhang, C.; Cui, Y.; Song, L.; Liu, X.; Hu, Z. Microwave assisted one-pot synthesis of graphene quantum dots as highly sensitive fluorescent probes for detection of iron ions and pH value. *Talanta* **2016,** *150*, 54-60.

(7) Atchudan, R.; Edison, T. N. J. I.; Aseer, K. R.; Perumal, S.; Karthik, N.; Lee, Y. R. Highly fluorescent nitrogen-doped carbon dots derived from Phyllanthus acidus utilized as a fluorescent probe for label-free selective detection of Fe^{3+} ions, live cell imaging and fluorescent ink. *Biosensors and Bioelectronics* **2018,** *99*, 303-311.

(8) Wang, L.; Bi, Y.; Hou, J.; Li, H.; Xu, Y.; Wang, B.; Ding, H.; Ding, L. Facile, green and clean one-step synthesis of carbon dots from wool: application as a sensor for glyphosate detection based on the inner filter effect. *Talanta* **2016,** *160*, 268-275.

(9) Song, Y.; Zhu, C.; Song, J.; Li, H.; Du, D.; Lin, Y. Drug-derived bright and color-tunable N-doped carbon dots for cell imaging and sensitive detection of Fe^{3+} in living cells. *ACS applied materials & interfaces* **2017,** *9* (8), 7399-7405.

(10) Nie, H.; Li, M.; Li, Q.; Liang, S.; Tan, Y.; Sheng, L.; Shi, W.; Zhang, S. X.-A. Carbon dots with continuously tunable full-color emission and their application in ratiometric pH sensing. *Chemistry of Materials* **2014,** *26* (10), 3104-3112.

(11) Zhang, Y.-Q.; Ma, D.-K.; Zhuang, Y.; Zhang, X.; Chen, W.; Hong, L.-L.; Yan, Q.-X.; Yu, K.; Huang, S.-M. One-pot synthesis of N-doped carbon dots with tunable luminescence properties. *Journal of Materials Chemistry* **2012,** *22* (33), 16714-16718.

(12) Zhi, B.; Cui, Y.; Wang, S.; Frank, B. P.; Williams, D. N.; Brown, R. P.; Melby, E. S.; Hamers, R. J.; Rosenzweig, Z.; Fairbrother, D. H. Malic acid carbon dots: from super-resolution live-cell imaging to highly efficient separation. *ACS nano* **2018,** *12* (6), 5741-5752.

(13) Kong, B.; Zhu, A.; Ding, C.; Zhao, X.; Li, B.; Tian, Y. Carbon dot-based inorganic–organic nanosystem for two-photon imaging and biosensing of pH variation in living cells and tissues. *Advanced materials* **2012,** *24* (43), 5844-5848.

(14) Liu, Q.; Guo, B.; Rao, Z.; Zhang, B.; Gong, J. R. Strong two-photon-induced fluorescence from photostable, biocompatible nitrogen-doped graphene quantum dots for cellular and deep-tissue imaging. *Nano letters* **2013,** *13* (6), 2436-2441.

(15) Tong, G.; Wang, J.; Wang, R.; Guo, X.; He, L.; Qiu, F.; Wang, G.; Zhu, B.; Zhu, X.; Liu, T. Amorphous carbon dots with high two-photon fluorescence for cellular imaging passivated by hyperbranched poly (amino amine). *Journal of Materials Chemistry B* **2015,** *3* (4), 700-706.

(16) Pan, L.; Sun, S.; Zhang, L.; Jiang, K.; Lin, H. Near-infrared emissive carbon dots for two-photon fluorescence bioimaging. *Nanoscale* **2016,** *8* (39), 17350-17356.

(17) Liu, J.; Dong, Y.; Ma, Y.; Han, Y.; Ma, S.; Chen, H.; Chen, X. One-step synthesis of red/green dual-emissive carbon dots for ratiometric sensitive $ONOO^-$ probing and cell imaging. *Nanoscale* **2018,** *10* (28), 13589-13598.
(18) Wang, H.; Di, J.; Sun, Y.; Fu, J.; Wei, Z.; Matsui, H.; del C. Alonso, A.; Zhou, S. Biocompatible PEG-chitosan@ carbon dots hybrid nanogels for two-photon fluorescence imaging, near-infrared light/pH dual-responsive drug carrier, and synergistic therapy. *Advanced Functional Materials* **2015,** *25* (34), 5537-5547.